Non-Gaussian time-dependent statistics of wind pressure processes on a roof structure

M.F. Huang[*], Song Huang, He Feng and Wenjuan Lou

Institute of Structural Engineering, Zhejiang University, Hangzhou 310058, China

Abstract. Synchronous multi-pressure measurements were carried out with relatively long time duration for a double-layer reticulated shell roof model in the atmospheric boundary layer wind tunnel. Since the long roof is open at two ends for the storage of coal piles, three different testing cases were considered as the empty roof without coal piles (Case A), half coal piles inside (Case B) and full coal piles inside (Case C). Based on the wind tunnel test results, non-Gaussian time-dependent statistics of net wind pressure on the shell roof were quantified in terms of skewness and kurtosis. It was found that the direct statistical estimation of high-order moments and peak factors is quite sensitive to the duration of wind pressure time-history data. The maximum value of COVs (Coefficients of variations) of high-order moments is up to 1.05 for several measured pressure processes. The Mixture distribution models are proposed for better modeling the distribution of a parent pressure process. With the aid of mixture parent distribution models, the existing translated-peak-process (TPP) method has been revised and improved in the estimation of non-Gaussian peak factors. Finally, non-Gaussian peak factors of wind pressure, particularly for those observed hardening pressure process, were calculated by employing various state-of-the-art methods and compared to the direct statistical analysis of the measured long-duration wind pressure data. The estimated non-Gaussian peak factors for a hardening pressure process at the leading edge of the roof were varying from 3.6229, 3.3693 to 3.3416 corresponding to three different cases of A, B and C.

Keywords: wind pressure; mixture distribution; non-Gaussian; peak factor; wind tunnel tests

1. Introduction

Many researchers have carried out investigations for the non-Gaussian statistics of wind pressure processes (Sadek and Simiu 2002, Tieleman *et al*. 2006, Kwon and Kareem 2011, Huang *et al*. 2013, Yang *et al*. 2013, Peng *et al*. 2014, Yu *et al*. 2014, Abhilash *et al*. 2014). Based on the translation process theory, two common approaches of translation methods are found in literatures. One type is based on the Hermite model and its variant; this type includes Kwon and Kareem's formula (2011), the approximate Hermite model expression proposed in Yang *et al*. (2013) and Peng *et al*. (2014). In this type of approach, the non-Gaussian properties of skewness γ_3 and kurtosis γ_4 are used. The second type of approach is based on the point-to-point cumulative distribution function (CDF) mapping procedure from non-Gaussian to Gaussian, with the Sadek–

Simiu (SS) procedure (2002) and the recently proposed translated-peak-process (TPP) method (Huang *et al*. 2013). Whereas the Sadek–Simiu procedure maps extreme values from the Gaussian space to the non-Gaussian space, the TPP method aims to properly model local peak distribution of non-Gaussian processes with the parametric Weibull distribution, from which the peak factor and the fractile level are obtained analytically. The TPP method has the same advantage as the Sadek–Simiu procedure because it makes use of all information contained in the time series. Furthermore, the TPP method provides the closed-form solution of peak factors. As long as the Weibull distribution parameters available, the peak factor and fractile levels of a non-Gaussian process can be analytically evaluated.

The possible improvement of the point-to-point mapping approach is the better modeling of parent wind pressure distributions. Recently, various mixture models have been proposed for the entire data distribution. One is so called multi-component mixture models, which make use of two or more component distributions to form a "mixed" or "compound" distribution. Bordes *et al.* (2006) developed a methodology for estimating unknown parameters in a two-component mixture model and the properties of the proposed estimators were illustrated by a Monte Carlo study. Akdag *et al.* (2010) applied the two-component mixture Weibull distribution to estimate wind speed characteristics for determining the annual mean wind power density. The other is the flexible extreme value mixture model (FEVMM), which simultaneously captures the bulk of the distribution (typically the main mode) with the flexibility of an extreme value model for the upper/lower tails (MacDonald *et al*. 2011a, b). Zheng *et al*. (2014) adapted mixture probability distributions to fit the wind pressure coefficients over the roof surface of low-rise buildings. The FEVMM has been used in translation methods to better estimate peak pressure effects (Peng *et al*. 2014, Ding and Chen 2014). However, the use of a mixture model may not offer a significant improvement over the existing translation methods (Peng *et al*. 2014). It is necessary to further investigate the effectiveness of the mixture models in the TPP method.

Hermite model–based approaches, including Kwon and Kareem's formula (Kwon and Kareem 2011), the work of Yang *et al*. (2013) and Peng *et al*. (2014) have inherent limits due to the use of the Hermite moment model developed by Winterstein (1988). The original Hermite moment model provides a representation of the functional transformation from a Gaussian process to a non-Gaussian softening process defined as the kurtosis γ_4 greater than 3 (Winterstein 1988). Most of existing Hermite model-based methods or formulas are therefore only applicable to a softening process with a positive excess kurtosis. In the Sadek-Simiu procedure, a gamma distribution was selected to model the parent distribution of a given pressure process. Because a gamma distribution has a positive excess kurtosis, it cannot be used to describe the parent distribution of a hardening process. To complete the original Hermite moment model for all practical paired values of skewness and kurtosis, several attempts have been made to extend the moment-based Hermite translation model for hardening non-Gaussian processes ($\gamma_4 - 3 < 0$) with empirical formulations for determining the translation model coefficients (Choi and Sweetman 2010, Chen 2014, Ding and Chen 2014). The modeling of translation function for hardening non-Gaussian wind effect processes has not been extensively addressed in literature (Chen 2014, Ding and Chen 2014). Huang *et al*. (2014) observed hardening wind pressure processes on a long-span roof model tested in the wind tunnel, and proposed an analytical formula for non-Gaussian peak factors of hardening load processes.

Based on the wind tunnel tests, the high-order moments, i.e., skewness and kurtosis, of the wind pressure processes measured on a double-layer reticulated shell roof are evaluated

statistically. According to the arrangements of coal piles inside the roof, three different cases are tested in the simulated atmospheric boundary layer winds. The paper work is derived from a practical project to assess wind-resistant structural design of a double-layer reticulated shell roof with a 120 m span through wind tunnel tests. The sensitivities of high-order statistics of wind pressure on the roof to the arrangement of coal piles are studied. The existing TPP method is revised by introducing two types of mixture distribution models to make better predictions of peak factors for non-Gaussian wind pressure processes. Comparative performance studies have been further carried out to reveal the advantage and disadvantage of various state-of-the-art translation methods, and investigate the effectiveness of mixture models in the TPP method. The main contribution of the paper is to reveal non-Gaussian time-dependent statistical properties of wind pressure on the roof and to develop new non-Gaussian wind pressure models for estimating peak wind loads more accurately. The new statistical property findings of wind pressure fields are important to understand dynamic wind load processes on the complex roof structure. The revised TPP method together with the proposed mixture non-Gaussian distribution models could be applied in wind engineering practices to better estimate peak wind loads on a complex building structure based on the limited wind tunnel test data.

2. Wind tunnel experiments

A cylindrical reticulated roof structure with a height of 45 m and a span of 120 m is planned to construct in a coastal site of China. The roof is as long as 240 m, and is open at two ends to store large amounts of coal piles for producing thermal power. The site is in the A category (open terrain), with a power law exponent of $\alpha=0.12$ for the mean wind speed profile stipulated in the Chinese Load Code (GB50009-2012). The turbulence intensity profile recommended for the A category is given by the following expression

$$I_u = I_{10}(\frac{Z}{10})^{-\alpha} \qquad (1)$$

where Z is the height, $I_{10}=0.12$. The simulated mean wind speed and turbulent profiles in the wind tunnel were provided in Fig. 1, where U_g is defined as the mean wind speed at a gradient height of 300 m for the A category site. It seems that the experimental curves of wind structures fit well with the theoretical ones.

Wind tunnel experiments were carried out in a boundary layer wind tunnel, which has a working cross section of 4 m wide × 3 m high and a length of 18 m. A model of the roof structure was made at a geometric scale of 1:150 by carefully mimicking the detailing of reticulated structural members as shown in Fig. 2. Three different testing cases were considered as the empty roof without coal piles (Case A of Fig. 2(a)), half coal piles inside (Case B of Fig. 2(b)) and full coal piles inside (Case C of Fig. 2(c)). It is noted that the cross section of coal piles (see Fig. 3) is designed according to the practice of thermal power industry in China. Spires and roughness cube elements were used to simulate the desired boundary layer wind structure following the A category. Wind pressures on the rigid model of the roof shell were measured using a synchronous multi-pressure sensing system (SMPSS). A total of 500 pressure sensors were densely distributed on the roof of the model to quantify the net pressure actions at 250 locations, as shown in Fig. 4.

(a) Mean wind speed profile   (b) Turbulent intensity profile
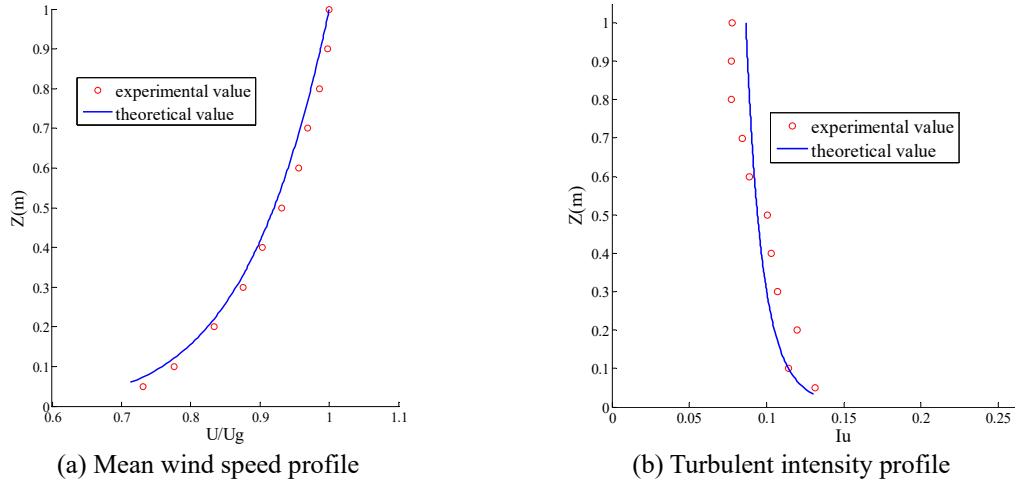
Fig. 1 Simulated wind field structures in wind tunnel tests

At each measuring site, a pair of pressure taps was installed to measure external and internal pressure effects simultaneously. The wind tunnel test was carried out with a wind speed of 15.4 m/s at the reference height of 1.0 m above the wind tunnel floor. The design wind speed with a return period of 100 years for the construction site is approximately 52.52 m/s at a full-scale height of 150 m. Therefore, the wind speed scale in the wind tunnel experiment was approximately 1/3.4 and the time scale became 1/44. Long-time duration pressure measurements were made for four typical wind angles of 0°, 30°, 45° and 90°, as defined in Fig. 4. The pressure data were recorded at a sampling frequency of 625 Hz for time duration of 300 s, which is equivalent to 220 minutes in full-scale situations.

The wind pressure results are presented in terms of the net pressure coefficient, which is defined as follows

$$C_{pi}(t) = \frac{P_i^{\text{ex}}(t) - P_i^{\text{in}}(t)}{0.5\rho V_\infty^2} \tag{2}$$

Where C_{pi} is the net pressure coefficient for the ith measuring position of the roof; P_i^{ex} and P_i^{in} are the pressure values at the external and internal surfaces of the roof, respectively. The main focus of this study is on the non-Gaussian and time-dependent characteristics of the wind pressure processes defined in Eq. (2).

Due to the sensitivity of the flow to Reynolds number for a curved surface, it is necessary to implement a certain level of surface roughness across the exterior of the roof model by simple paper strips as shown Fig. 5. The Reynolds number for the roof model during wind tunnel test is about 8.2×10^5, which is greater than the critical Reynolds number of 2×10^5 for a smooth cylinder (Butt *et al.* 2014). Therefore, the wind pressure results in the wind tunnel tests can be applied to the real turbulent wind conditions.
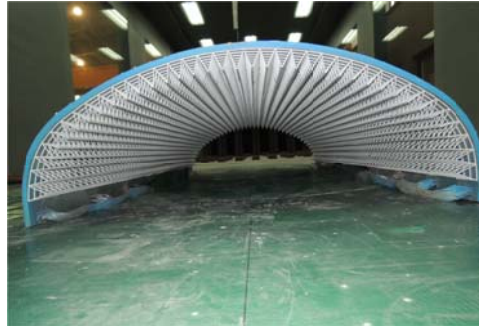
(a) Case A: Empty roof

(b) Case B: Half coal piles
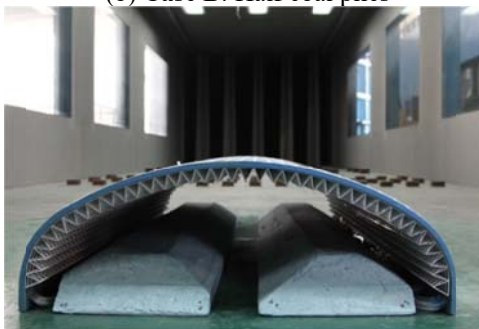
(c) Case C: Full coal piles
Fig. 2 Wind tunnel test models of a double-layer reticulated shell
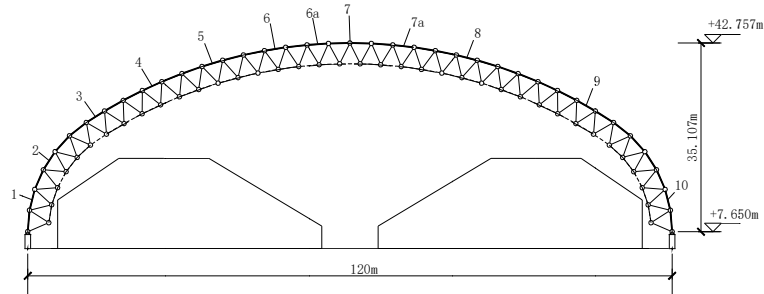
Fig. 3 Arrangements of pressure taps along the cross section of the shell roof
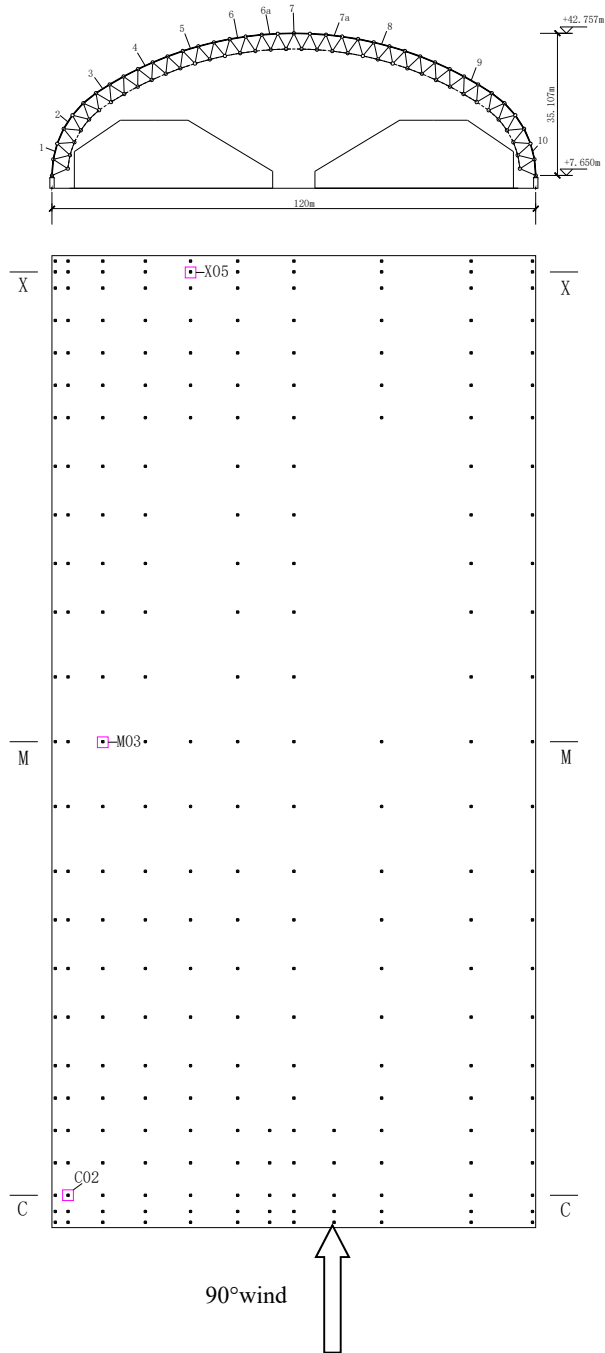
Fig. 4 Arrangements of pressure taps on the shell roof
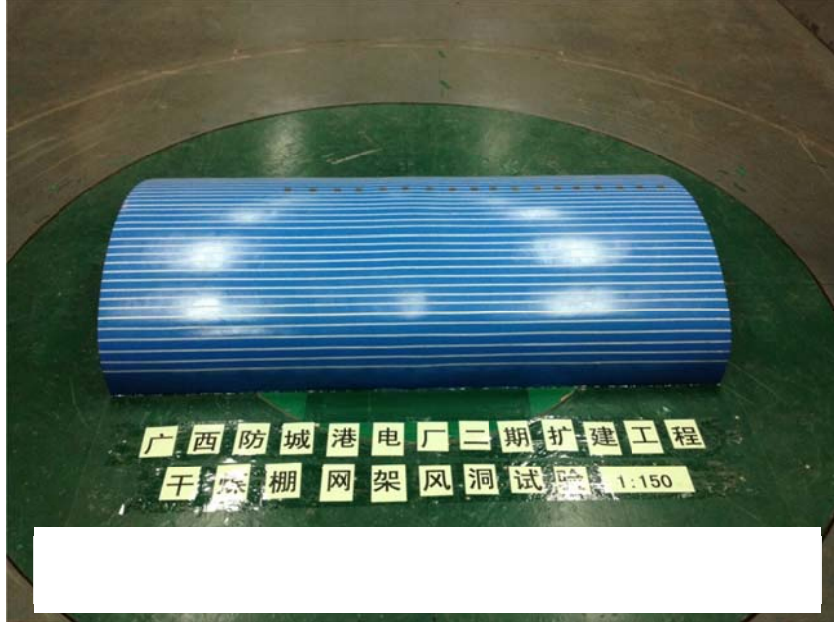
Fig. 5 The surface roughness on the wind tunnel test model of a double-layer reticulated shell

3. High order statistics of long duration wind pressure

Skewness and kurtosis are the two main parameters used to measure non-Gaussian characteristics for a given process. For the data sample of pressure coefficients with N data points sampled at discretized time instants t_j, $j=1,...,N$, the skewness and kurtosis can be estimated statistically as follows

$$\gamma_3 = \frac{1}{N} \sum_{j=1}^{N} \left[\frac{C_{pi}(t_j) - C_{pi,\text{mean}}}{C_{pi,\text{std}}} \right]^3 \tag{3}$$

$$\gamma_4 = \frac{1}{N} \sum_{j=1}^{N} \left[\frac{C_{pi}(t_j) - C_{pi,\text{mean}}}{C_{pi,\text{std}}} \right]^4 \tag{4}$$

where $C_{pi,mean}$ and $C_{pi,std}$ are the mean and standard deviation, respectively, of the pressure coefficient.

As reported by Choi and Sweetman (2010), a skewness–kurtosis combination for a random process will satisfy the following practical limit

$$\gamma_4 \geq \gamma_3^2 + 1 \tag{5}$$

The monotonic region, which defines the applicable range for the application of the Hermite

polynomial model, could be expressed as (Winterstein and MacKenzie 2012)

$$\gamma_4 \geq \left(1.25\gamma_3\right)^2 + 3 \tag{6}$$

It is clear that γ_4 should be greater than 3. Therefore, the Hermite polynomial model (HPM) proposed in the work of Yang *et al.* (2013) and Peng *et al.* (2014) is only applicable for softening non-Gaussian processes. Fig. 6 presents a scatter plot of paired values of skewness and kurtosis in moment space for all measured long-time duration net pressure coefficients at four angles (0°, 30°, 45° and 90°) of three cases (A, B and C). Therefore, total 250×4×3=3000 data points were plotted in Fig. 6. The colors of each point in the scatter plot were randomly selected by Matlab program to distinguish the data points from each other. While the parabolic dashed curve shown in Fig. 6 represents the practical limit given by Eq. (5), the parabolic solid curve indicates the monotonic region of Eq. (6). As shown in Fig. 6, the skewness–kurtosis combinations of all measured net pressure coefficients on the roof are above this parabolic limit. As expected, a small number of points fall out of the monotonic region and below the line of $\gamma_4 = 3$, indicating the occurrence of hardening wind pressure processes are relatively rare.

The contours of skewness and kurtosis of the wind pressure field are presented in Figs. 7 and 8 for three cases under 90° wind. Fig. 7 shows that the patterns of skewness distributions are more or less the same for three test cases. On the other hand, the presence of coal piles inside the roof seems to change the distribution patter of kurtosis contours. Under the wind angle of 90°, the wind flows pass through the empty roof easily. For the other two cases of half and full coal piles, wind flows inside the roof would be disturbed by coal obstacles. Especially for the case of half coal piles, which are placed at the middle position along the long direction of the roof, wind flow would break away from the surface of the coal obstacles. Once this separation occurs, the wind flow inside the roof might form unsteady and recirculating vortices.
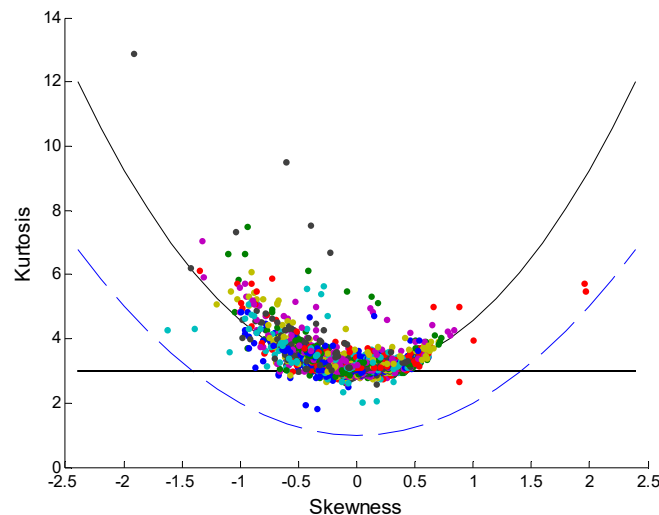

Fig. 6 Paired values of skewness and kurtosis
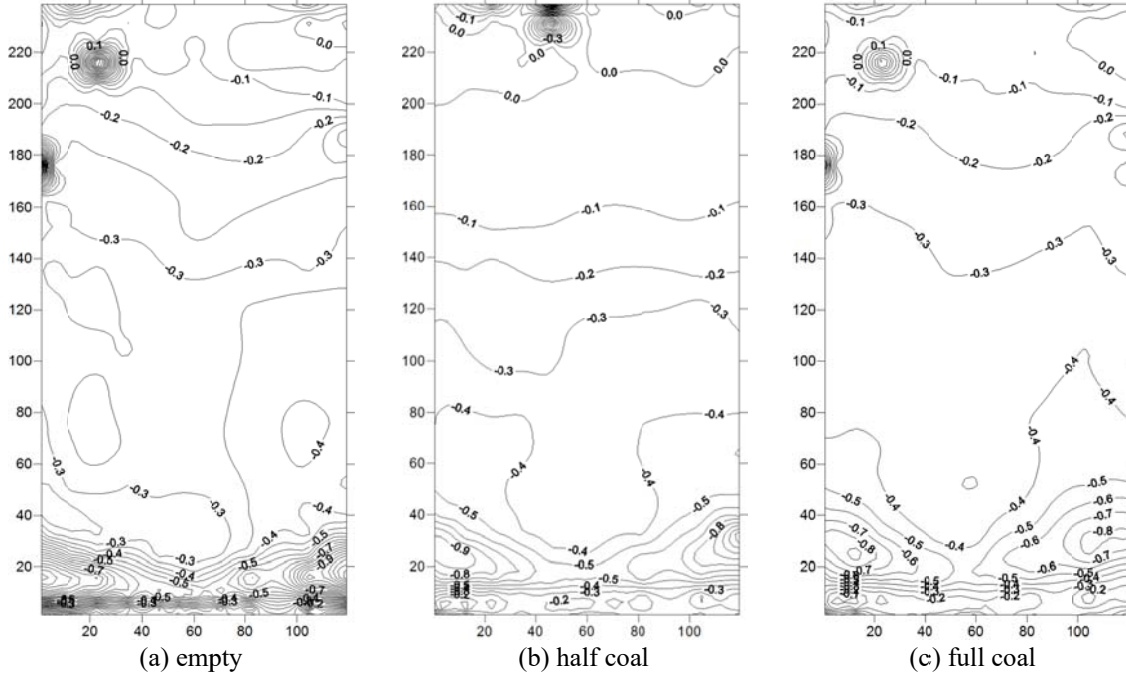
Fig. 7 Skewness contours under 90° wind for three coal arrangement cases
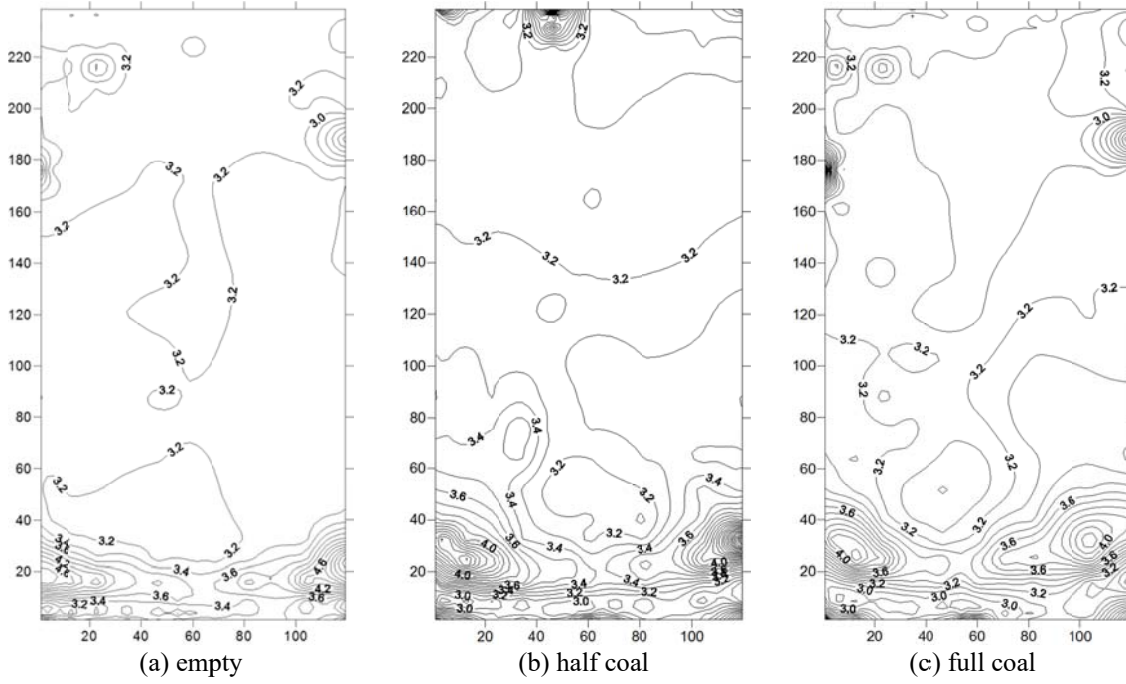
Fig. 8 Kurtosis under 90° wind for three coal arrangement cases

(a) C cross-section

(b) M cross-section
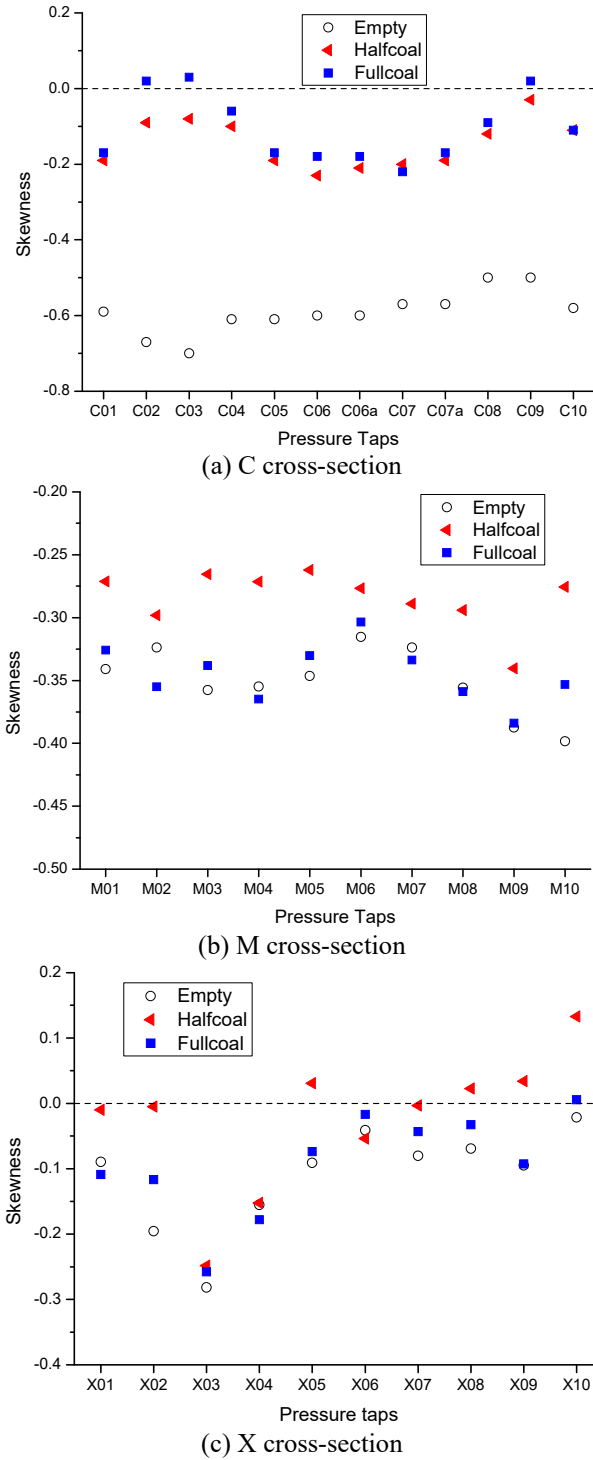
(c) X cross-section

Fig. 9 Skewness of pressure processes along the cross sections of the roof under 90° wind

(a) C cross-section

(b) M cross-section
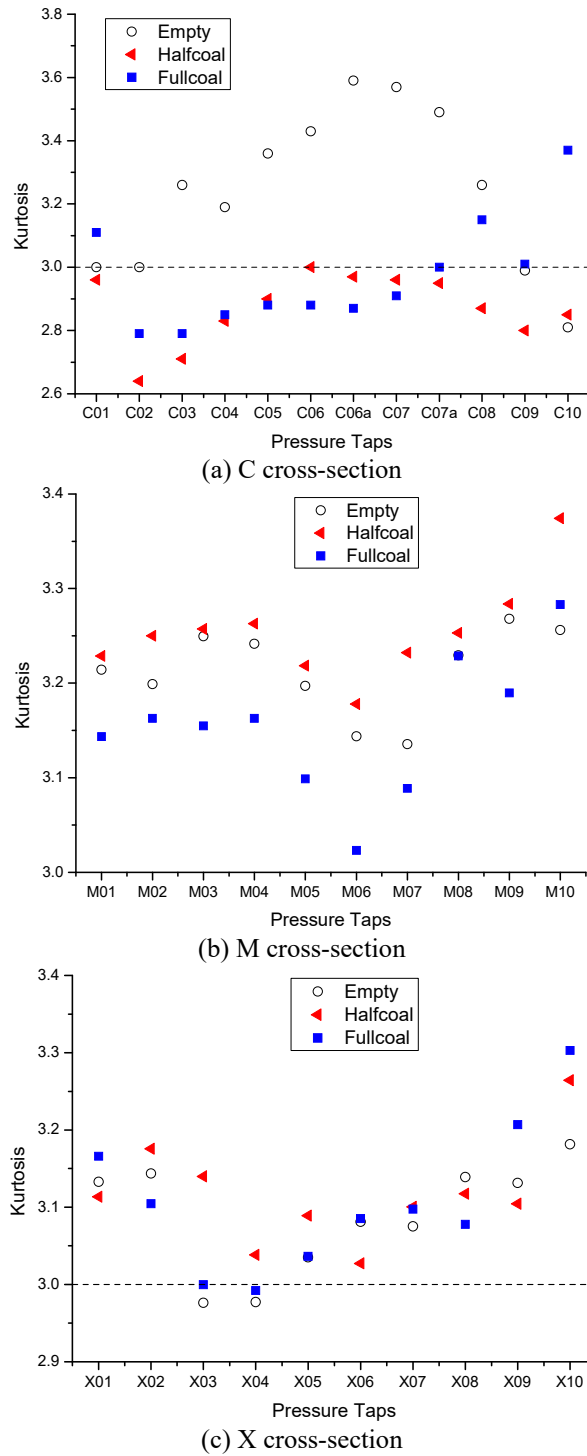
(c) X cross-section

Fig. 10 Kurtosis of pressure processes along the cross sections of the roof under 90° wind

The effect of coal obstacles on the high-order statistics of wind pressure was also studied along three typical cross sections of the roof, i.e., the leading edge C cross section, the middle M cross section and the outlet X cross section. It was found from Fig. 9(a) that the negative skewness of -0.7 for the empty roof was changed to be -0.1 for two other cases at the measuring sites of C02 and C03. Such a substantial change might be due to the block of wind flow by coal obstacles when wind starts to enter the roof. Along the middle M cross section and the outlet X cross section as shown in Figs. 9(b) and 9(c) and Figs. 10(b) and 10(c), the effect of coal obstacles on the values of skewness and kurtosis becomes smaller compared to the leading edge C cross section.
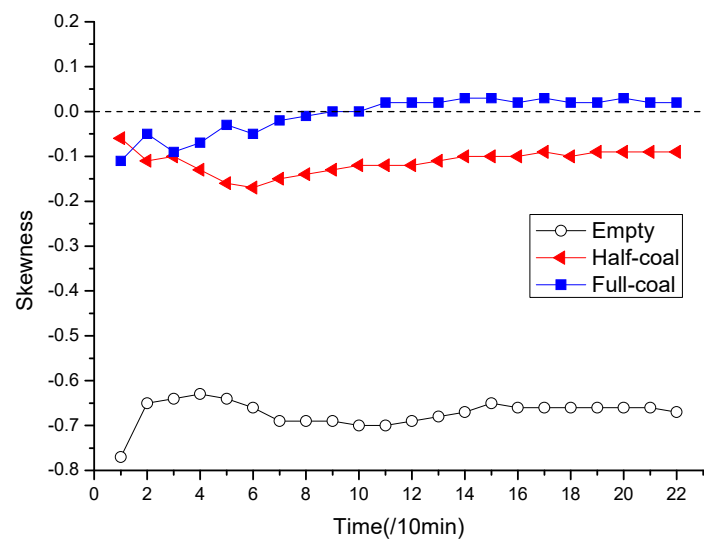

(a)
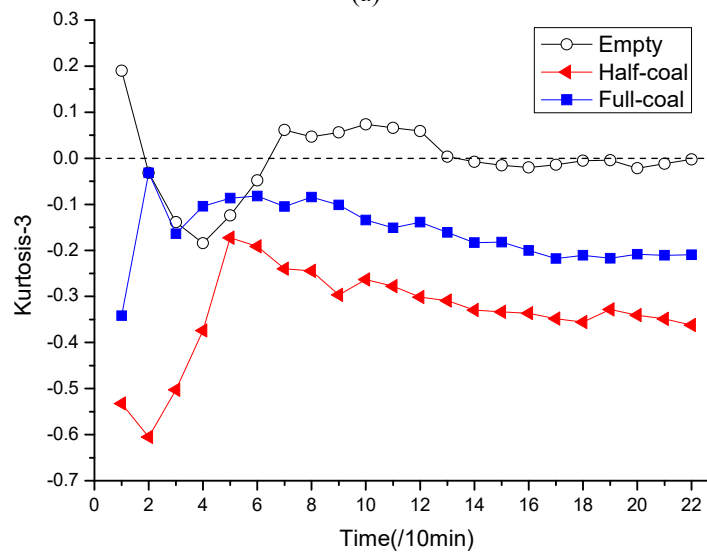
(b)

Fig. 11 Estimated time-dependent skewness and kurtosis for C02 under 90° wind

The sensitivities of skewness and kurtosis to the record duration were presented in Figs. 11-13. Each data point in Figs. 11-13 is an estimation based on increasing data record with a 10-miniute step. Figs. 11-13 present high-order moments for three typical net pressure processes, measured at the pressure tap sites, i.e., C02, M03 and X05 (denoted as square in Fig. 4) under 90° wind. The estimated values of skewness and kurtosis are obviously fluctuated with the varying record duration. The dispersion of the estimated high-order moments could be measured by the coefficients of variations (COVs), which is defined by the standard deviation (STD) of the estimator over its mean. Table 1 summaries the results of COVs for high-order moments of pressure processes measured at sites of C02, M03 and X05 under wind. The estimated higher statistical moments generally have large variations, i.e., greater than 0.1, especially when the process is of strongly non-Gaussian properties. It should be noted that the COV results in the bracket were calculated with the absolute values of the estimator, otherwise the almost zero mean may cause too large COV, i.e., much greater than 1. Such significant COV results of skewness and kurtosis indicate that high-order moments of non-Gaussian pressure processes might become non-stationary.

(a)

(b)
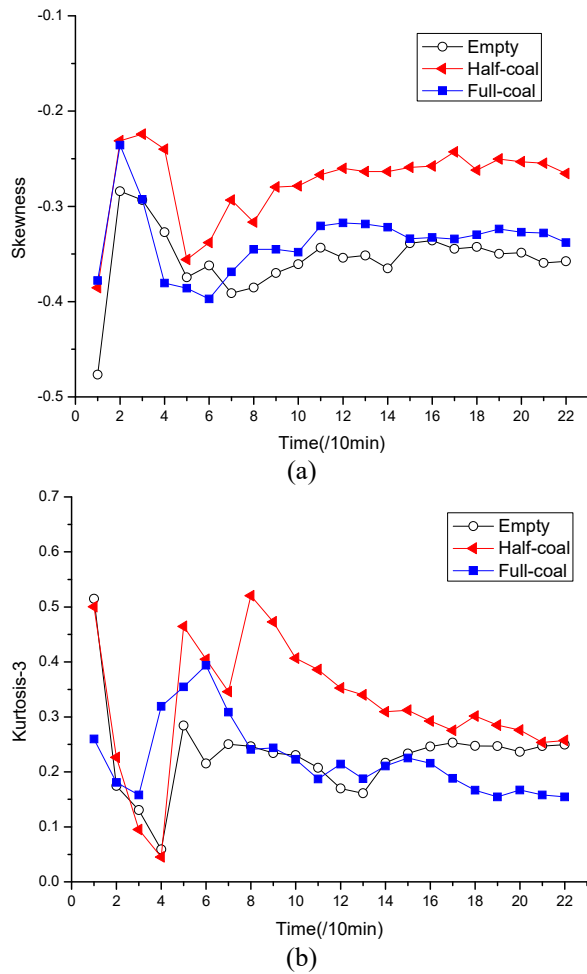
Fig. 12 Estimated time-dependent skewness and kurtosis for M03 under 90° wind
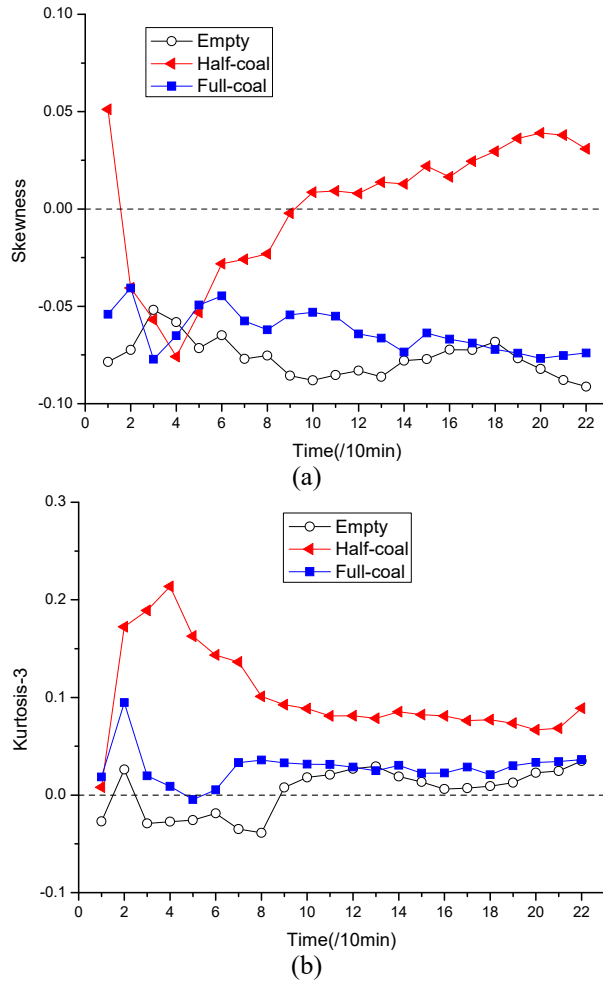
Fig. 13 Estimated time-dependent skewness and kurtosis for X05 under 90° wind

Table 1 COV of high-order moments for pressure processes on the roof under 90° wind

		Empty	Half coal	Full coal
C02	Skewness	-0.04	-0.23	(0.84)
	Kurtosis-3	(1.05)	-0.30	-0.42
M03	Skewness	-0.10	-0.15	-0.10
	Kurtosis-3	0.35	0.36	0.30
X05	Skewness	-0.13	(0.62)	-0.17
	Kurtosis-3	(0.43)	0.47	0.64

4. Mixture models for parent pressure distribution

4.1 Flexible extreme value mixture model (FEVMM)

The point-to-point CDF mapping approaches, i.e., the TPP methods, require the parent distribution models. In this paper, two types of mixture distribution models were used for analyzing the parent wind pressure data. The FEVMM includes a non-parametric smooth kernel density estimator below some threshold accompanied with the generalized Pareto distribution (GPD) model for the upper tail above the threshold. This mixture model avoids the need to assume a parametric form for the bulk distribution, and captures the entire distribution function below the threshold using a smooth flexible non-parametric form. The expression for GPD is

$$F_{GPD}(x) = \Pr(X \leq x | X > u) = \frac{F_X(x) - F_X(u)}{1 - F_X(u)} = 1 - \left[1 + \frac{\xi(x-u)}{\sigma}\right]^{-1/\xi} \tag{7}$$

where u denotes the chosen threshold; σ and ξ are scale and shape parameters, respectively. When $\xi = 0$, the GPD becomes exponential distribution. The inference of GPD parameters can be performed using either maximum likelihood or method of moments applied to the data beyond the selected tail-index u (Harris 2005). The GPD model provides an approximation to parent CDF above a selected high threshold u as

$$F_X(x) = F_X(u) + F_{GPD}(x)\left[1 - F_X(u)\right], \quad x \geq u \tag{8}$$

The corresponding probability density function (PDF) of Eq. (8) can be denoted as KP-pdf. The original version of the TPP method can be modified by adopting the proposed mixture model for parent pressure distribution. The modified version was denoted as ParTPP for comparison purposes.

4.2 Multi-component mixture models

In a mathematical sense, a random variable has a finite mixture distribution, if its distribution can be represented by a probability density function (PDF) of the form

$$f(x) = p_1 f_1(x | \theta_1) + p_2 f_2(x | \theta_2) + ... + p_k f_k(x | \theta_k)$$

$$p_i \geq 0, f_i(x | \theta_i) \geq 0, \int f_i(x | \theta_i) dx = 1, i = 1, 2, ..., k, \sum_{i=1}^{k} p_i = 0 \tag{9}$$

where $f_i(x | \theta_i)$ is the component density of the mixture; k is the number of components that constitute the mixture; the parameters $p_1, p_2, ..., p_k$ are the mixing weights and $\theta_1, \theta_2, ..., \theta_k$ are the parameters of each component distribution. In this work, the mixture consists of two components and each component density function is either a normal distribution or a well-known two-parameter Weibull density function. Consequently, the mixture density can be expressed as:

$$f(x | \theta) = p f_1(x | \theta_1) + (1 - p) f_2(x | \theta_2) \tag{10}$$

When considering a mixture of double Weibull, the mixture density distribution can be defined as WW-pdf

$$f(x\,|\,k_1,c_1,k_2,c_2,p) = p\{\frac{k_1}{c_1}(\frac{x}{c_1})^{k_1-1}\exp[-(\frac{x}{c_1})^{k_1}]\} + (1-p)\{\frac{k_2}{c_2}(\frac{x}{c_2})^{k_2-1}\exp[-(\frac{x}{c_2})^{k_2}]\} \quad (11)$$

where the parameters k_1, k_2 and c_1, c_2 are called shape parameters and scale parameters, respectively. If considering a mixture of normal and Weibull, the mixture density distribution becomes NW-pdf:

$$f(x\,|\,k_1,c,\mu,\sigma,p) = p\{\frac{k_1}{c_1}(\frac{x}{c_1})^{k_1-1}\exp[-(\frac{x}{c_1})^{k_1}]\} + (1-p)\{\frac{1}{\sqrt{2\pi}\sigma}\exp[-\frac{(x-\mu)^2}{2\sigma^2}]\} \quad (12)$$

where μ and σ are the mean and standard deviation of the normal distribution. The maximum likelihood method is applied in the present study to estimate the values of the parameters, which maximize the function of log-likelihood. For two-component Weibull mixtures, the function of log- likelihood can be defined as

$$\ln L(x_1,...,x_n\,|\,k_1,c_1,k_2,c_2,p) = \ln\prod_{i=1}^{n}\left\{ p\{\frac{k_1}{c_1}(\frac{x_i}{c_1})^{k_1-1}\exp[-(\frac{x_i}{c_1})^{k_1}]\} + (1-p)\{\frac{k_2}{c_2}(\frac{x_i}{c_2})^{k_2-1}\exp[-(\frac{x_i}{c_2})^{k_2}]\} \right\}$$

$$= \sum_{i=1}^{n}\ln\left\{ p\{\frac{k_1}{c_1}(\frac{x_i}{c_1})^{k_1-1}\exp[-(\frac{x_i}{c_1})^{k_1}]\} + (1-p)\{\frac{k_2}{c_2}(\frac{x_i}{c_2})^{k_2-1}\exp[-(\frac{x_i}{c_2})^{k_2}]\} \right\} \quad (13)$$

The Newton-Raphson algorithm can be used to maximize the above log-likelihood function (Titterington *et al.* 1995).

4.3 The goodness-of-fit for mixture models

Fig. 14 presents wind pressure histograms from observed data together with NW-pdf, WW-pdf and KP-pdf, for pressure processes measured at C02 under 90° wind. It can be seen the proposed mixture distribution models seem to fit well with the histograms, even in cases that wind pressure data set does not show a bimodal distribution. Table 2 lists the empirical values of the distribution parameters (e.g., k_1,k_2,c_1,c_2) and the mixing weight p of the mixture models for C02 under 90° wind. It was found that the mixing weight values for both NW-pdf and WW-pdf are greater than 0.1, indicating the significance of "compound" in these two mixture models. The empirical values of the parameters of the FEVMM and single Weibull were reported in Table 3.

The goodness-of-fit of a statistical model describes how well it fits a set of observations. In this paper, three commonly used statistical tests are used to evaluate the fitness of various mixture models. The probability plot correlation coefficient (PPCC) test developed by Filliben (1975) is known a simple and powerful goodness-of-fit test. The test statistic is the correlation coefficient r between the ordered observations x_i and the corresponding fitted quantiles m_i determined by the proposed probability distribution models. If the assumption that the observations could have been drawn from the fitted distribution is true, the value of r is close to unity. The correlation coefficient r is defined by (Filliben 1975)

(a) Empty roof

(b) Half coal piles

(c) Full coal piles
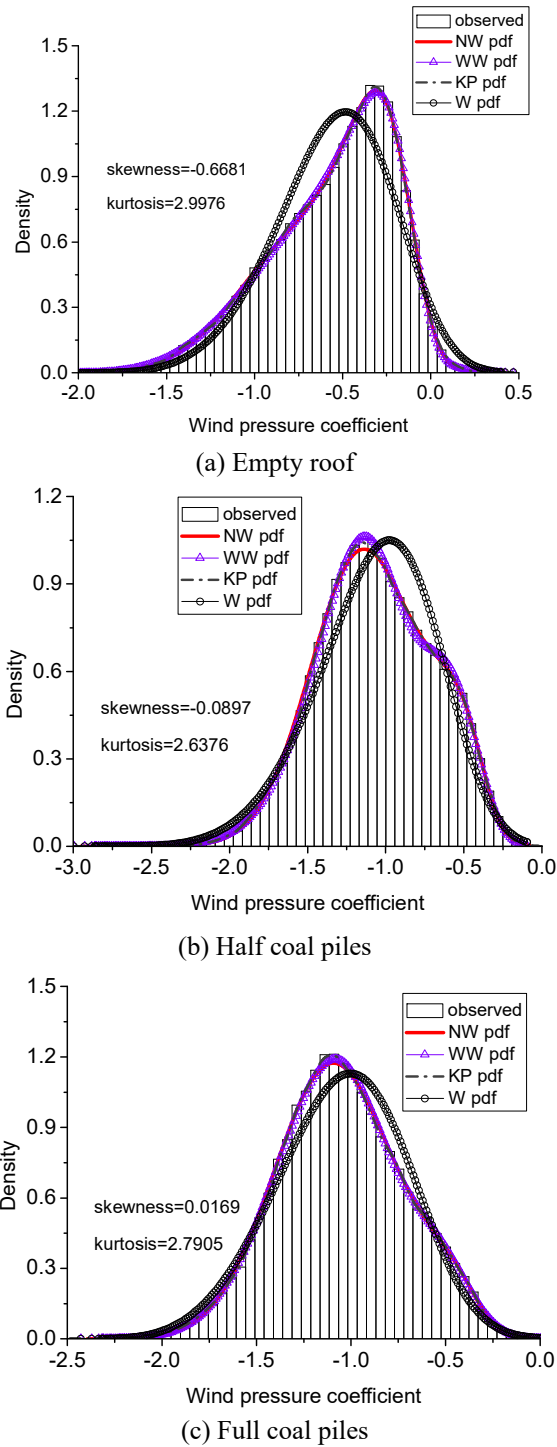
Fig. 14 The PDF of pressure process at C02 under 90° wind

Table 2 Emprical values of the parameters of the two mixture models

Site	Case	NW-PDF					WW-PDF				
		k	c	μ	σ	p	k_1	c_1	k_2	c_2	p
	Empty	1.82	10.03	1.31	0.35	0.54	1.84	11.05	1.50	4.35	0.43
C02	Half-coal	2.42	13.62	1.79	0.33	0.19	2.33	10.36	1.80	7.27	0.38
	Full-coal	1.90	11.24	1.30	0.31	0.15	1.80	7.96	1.33	5.21	0.26

Table 3 Emprical values of the parameters of KP-PDF and single Weibull

Site	Case	KP-PDF			Weibull	
		ξ	σ	u	k	c
	Empty	0.09	0.06	2.22	1.67	5.33
C02	Half-coal	-0.22	0.05	2.72	2.04	5.75
	Full-coal	0.00	0.05	2.19	1.48	4.41

$$r = \frac{\sum_{i=1}^{n}(x_i - \bar{x})(m_i - \bar{m})}{\sqrt{\sum_{i=1}^{n}(x_i - \bar{x})^2 \sum_{i=1}^{n}(m_i - \bar{m})^2}} \tag{14}$$

where $\bar{x}$ and $\bar{m}$ are the mean values of the observations and the fitted quantiles, respectively. The Kolmogorov-Smirnov test (K-S) is also used to decide if a sample comes from a population with a specific distribution. The KS indicator is defined as the maximum error in cumulative distribution functions

$$KS = \max_i \left| \hat{F}_i - F_i \right| \tag{15}$$

where F_i is the empirical distribution function of the observations; $\hat{F}_i$ is the fitted theoretical cumulative distribution function. Lesser KS value indicates better fitness. Another measure of fitness is the root mean squared error (RMSE), which provides a term-by-term comparison of the actual deviation between the empirical and fitted probabilities. A lower value of RMSE indicates a better distribution function model. The RMSE is defined as

$$\text{RMSE} = \left[\frac{1}{n} \sum_{i=1}^{n} \left(\hat{F}_i - F_i \right)^2 \right]^{1/2} \tag{16}$$

Table 4 Tests of goodness-of-fit for mixture models applied to pressure processes at C02 under 90° wind

Cases	PDF	C02		
		PPCC	KS	RMSE
Empty roof	NW	0.99997	0.00314	0.00107
	WW	0.99996	0.00372	0.00126
	KP	0.99999	0.00376	0.00095
	W	0.99298	0.05674	0.02130
Half coal	NW	0.99989	0.00470	0.00150
	WW	0.99994	0.00371	0.00128
	KP	1.00000	0.00199	0.00077
	W	0.99591	0.03844	0.01443
Full coal	NW	0.99991	0.00433	0.00163
	WW	0.99991	0.00422	0.00140
	KP	1.00000	0.00209	0.00074
	W	0.99792	0.03041	0.01181

Table 4 shows the tests of goodness-of-fit for mixture models applied to pressure processes at C02 under 90° wind. Generally, mixture models have smaller KS and RMSE values compared to the single Weibull model. The PPCC values of mixture models are also very close to 1.0. Based on the test results of goodness-of-fit, the mixture models should be the better choices for modeling the PDFs of asymmetric distribution or strongly non-Gaussian pressure processes.

5. Non-Gaussian peak factors

5.1 The CDF mapping approach

For a zero-mean process, the so-called peak factor can be defined as the ratio of the mean extreme value to the standard deviation value of the process. Different methods were employed in this paper to calculate peak factors of wind pressure processes. The SS procedure, the TPP method and its revised version represent the common CDF mapping approach. The detail of the TPP method can be referred to the work (Huang *et al*. 2013). Here, the main procedure of the TPP method was provided. In the TPP method, the mean extreme of a given non-Gaussian process $X(t)$ is calculated by the so called Weibull peak factor as

$$g_W = \left[\rho \ln \left(v_0 T \right) \right]^{1/\kappa} + \frac{\gamma \left[\rho \ln \left(v_0 T \right) \right]^{1/\kappa}}{\kappa \ln \left(v_0 T \right)}$$

(17)

where κ, ρ = the shape parameter and the scale parameter of the peak Weibull distribution, respectively; γ = Euler's constant (≈ 0.5772); ν_0 = the mean zero upcrossing rate of the non-Gaussian process; T= time duration. When $\kappa = 2$ and $\rho = 2$, Eq. (17) is reduced to the classical Davenport's peak factor as

$$g_W = \sqrt{2\ln(\nu_0 T)} + \gamma / \sqrt{2\ln(\nu_0 T)} \tag{18}$$

The peak distribution of the given non-Gaussian pressure process was modelled by the two-parameter Weibull distribution, which was empirically determined by a translation procedure from peaks of a Gaussian process to the peaks of the non-Gaussian process. The mapped peak data of the non-Gaussian process are then fitted to the Weibull distribution to determine the scale and shape parameters required by Eq. (17). The translation procedure to generate the peaks of the non-Gaussian process is executed with the following steps:

(a) Select a probability value (between zero and one) for the cumulative distribution function

(CDF) $F_{Y_m}(y_{pk}) = P(Y_m \leq y_{pk}) = 1 - \exp\left[-\frac{1}{2}(y_{pk})^2\right]$, which is the Rayleigh distribution

for peaks Y_m of a standardized Gaussian process.

(b) Find the corresponding peak value y_{pk} through the Rayleigh distribution.

(c) Find the corresponding Gaussian distribution function value $\Phi(y_{pk})$ at the peak y_{pk}.

(d) With $\Phi(y_{pk}) = F_x(x_{pk})$ determine the corresponding value of non-Gaussian peak x_{pk}, where $F_x(x)$ is the CDF of the non-Gaussian process *x(t)*.

(e) The desired point on the CDF $F_{X_m}(x_{pk})$ of the non-Gaussian peaks X_m can be obtained from the abscissa of the non-Gaussian peak x_{pk} and the ordinate with $F_{X_m}(x_{pk}) = F_{Y_m}(y_{pk})$.

(f) Repeat steps (a)~(e) by assigning an increased probability value of $F_{Y_m}(y_{pk})$ to generate the CDF of the peaks X_m for the given non-Gaussian process *x(t)*.

The above TPP procedure require the information of the parent CDF, which may be empirically obtained by using various methods or models, including the kernel-smoothing method (Hastie *et al*. 2009), the FEVMM, and the two-component mixture models. For comparison, the original TPP method with the kernel-smoothing estimator, the TPP method with the FEVMM, and the TPP method with the mixture models are denoted as TPP, parTPP and mixTPP, respectively.

5.2 The Hermite model approach

The Hermite model approach was implemented by employing two non-Gaussian peak factors for softening processes and hardening processes, respectively. For a softening process, Kwon and Kareem (2011) revisited the non-Gaussian peak factor and developed the following expression of the Hermite moment-based non-Gaussian peak factor (Kareem and Zhao 1994, Kwon and Kareem 2011)

$$\overline{x}_{ng} = \alpha \{ \left(\beta + \frac{\gamma}{\beta} \right) + h_3 (\beta^2 + 2\gamma - 1 + \frac{1.98}{\beta^2})$$

$$+ h_4 [\beta^3 + 3\beta(\gamma - 1) + \frac{3}{\beta}(\frac{\pi^2}{6} - \gamma + \gamma^2) + \frac{5.44}{\beta^3}]\}$$
(19)

where $\beta = \sqrt{2\ln(\nu_0 T)}$; ν_0 = mean zero upcrossing rate of a standardized non-Gaussian process $x(t)$ (obtained from a general non-Gaussian process $X(t)$ as $x(t) = [X(t) - \mu_X]/\sigma_X$, where μ_X =mean value of X(t), σ_X = the standard deviation of $X(t)$); α, h_3, h_4 are parameters of the moment-based Hermite model (Winterstein 1988), which gives a transformation from a standard Gaussian process $y(t)$ to the standardized non-Gaussian process $x(t)$

$$x = \alpha \left[y + h_3 (y^2 - 1) + h_4 (y^3 - 3y) \right]$$
(20)

where the parameters h_3 and h_4 control the shape of the distribution, while the parameter $\alpha = (1 + 2h_3^2 + 6h_4^2)^{-1/2}$ is the scaling factor. In the "softening" case, that is, $\gamma_4 > 3$, the second-order and third-order approximate analytical solutions are available (Winterstein 1988, Winterstein and Kashef 2000). New expressions for h3 and h4 were recently suggested by Yang *et al.* (2013)

$$h_3 \approx 0.1967\gamma_3 - 0.01646\gamma_3\gamma_4 + 0.01809\gamma_3^3$$
(21)

$$h_4 \approx -0.0721 + 0.03176\gamma_4 - 0.02942\gamma_3^2 - 0.00179\gamma_4^2 + 0.002348\gamma_3^2\gamma_4$$
(22)

Eqs. (19), (21), (22) establish a way to evaluate non-Gaussian peak factors of softening processes, denoted as NGS.

Based on the work of Choi and Sweetman (2010), an analytical solution for the non-Gaussian peak factor of a hardening process can be obtained as (Huang *et al.* 2014)

$$g_{NGH} = \frac{-h_3}{3h_4} + \frac{1}{3}\sqrt{3a_1 - a_2^2} \times \left[\left(C_0 + \sqrt{C_0^2 + 1} \right)^{1/3} - \left(C_0 + \sqrt{C_0^2 + 1} \right)^{-1/3} \right]$$
(23)

where $a_1 = (1 - 3h_4)/h_4, a_2 = h_3/h_4$ and C_0 are three parameters depending only on the Hermite coefficients h_3 and h_4; C_0 is given as follows

$$C_0 = \frac{-27(-\beta - \gamma/\beta - h_3)/h_4 + 9a_1a_2 - 2a_2^3}{54} \times \left(\frac{9}{3a_1 - a_2^2} \right)^{1.5}$$
(24)

The use of Eq. (23) to calculate the non-Gaussian peak factor of a hardening process is denoted as NGH.
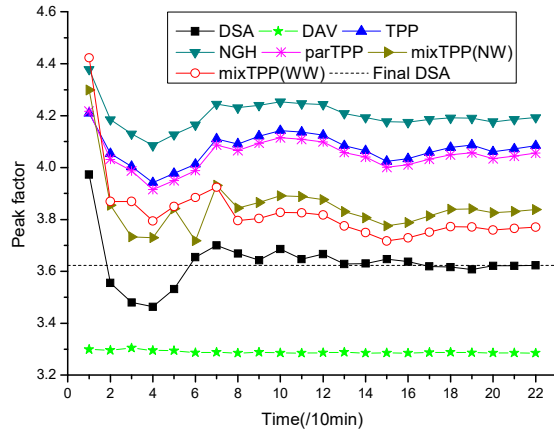
(a) Empty roof (Skewness=-0.6681, Kurtosis=2.9976)
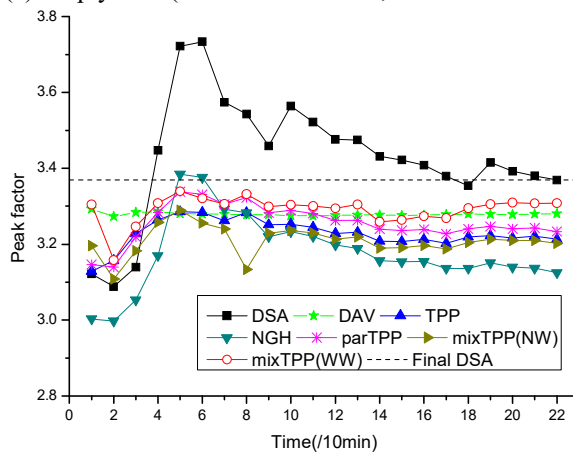
(b) Half coal piles (Skewness=-0.0897, Kurtosis=2.6376)
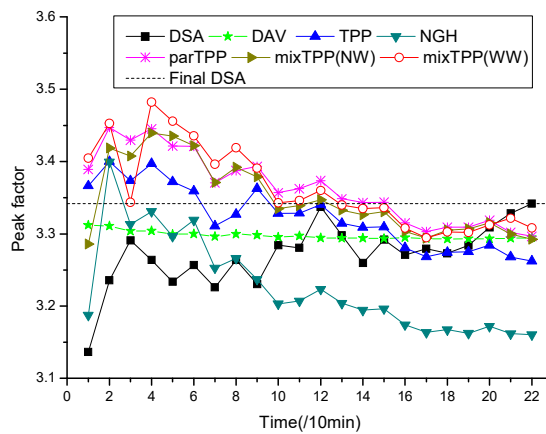
(c) Full coal piles (Skewness=0.0169, Kurtosis=2.7905)

Fig. 15 Comparison of estimated peak factors of pressure process at C02 under 90° wind

Table 5 The percentage errors of calculated peak factors compared with results of final DSA for C02

Methods	Cases		
	Empty roof	Half coal	Full coal
DAV	-9.33%	-2.64%	-1.41%
NGH	15.74%	-7.25%	-5.43%
TPP	12.73%	-4.63%	-2.37%
parTPP	11.95%	-4.03%	-1.35%
mixTPP(NW)	5.95%	-4.94%	-1.48%
mixTPP(WW)	4.05%	-1.82%	-1.00%

6. Results and discussions

The peak factor results were respectively calculated by five methods, i.e., DAV (Davenport's peak factor), TPP, ParTPP, MixTPP and NGS (or NGH). The total duration of pressure time history data for direct statistical analysis was 220-minute in full-scale, including 22 samples of 10-minute pressure coefficient data. The expected maximum (peak factor) of pressure coefficients for 10-minute duration were then computed by averaging the 22 observed maximum pressure coefficients over the 22 samples of 10-minute records. The direct statistical analysis (DSA) could provide benchmark results for weighting up other methods.

Fig. 15 presents non-Gaussian peak factors of pressure processes from C02 under 90° wind for three cases. The 22 peak factor results were obtained with varying record duration corresponding to each method. That is to say, the data used for calculating peak factors is starting from the first 10-minute duration to two 10-minute durations, up to 220-minute duration. For the empty case, the NGH largely overestimated the peak factors compared to the DSA benchmark results. The CDF mapping approach (i.e., TPP, parTPP and mixTPP) seems to have better performance in the estimation of non-Gaussian peak factors. While the parTPP just slightly improves the peak factor results, the mixTPP (WW) is capable of obtaining the best peak factor predictions with a small 4% overestimation compared to the final DSA of 3.6229. It was noted that the Davenport's peak factor underestimated the peak factors due to the asymmetric distribution of the pressure process (i.e., skewness is up to -0.6681) under consideration.

For the half-coal case, the pressure process with a kurtosis of 2.6376 is a hardening process. Various methods seem to all underestimated the peak factors compared to the final DSA of 3.3693. The mixTPP (WW) is also able to slightly improve the estimation of peak factors compared to the original TPP method. The DSA results of peak factors exhibit noticeable fluctuations indicating the possible non-stationary property of peak factor for a hardening process, which may cause the difficulty to adequately determinate peak wind loads in practice and needs to be better explained through a future study. The similar fluctuation in the estimation of peak factors was also observed for the full-coal case. The percentage errors of calculated peak factors compared with results of final DSA were reported in Table 3 for C02 under 90° wind. The TPP type methods are able to achieve better predictions of peak factors with percentage errors less than 5% (see Table 3)

compared to the moment-based translation method, i.e., NGH. Actually, the accuracy of the moment-based translation method is largely depending on the reliable estimation of skewness and kurtosis. For strongly non-Gaussian processes, the stable estimation of skewness and kurtosis is not guaranteed even using long duration pressure time histories since high-order moments might become non-stationary. The comparison of peak factor results could lead to a conclusion that the mixTPP method using two-component Weibull mixtures shows noticeable improvement over the original TPP method in the calculation of peak factors for strongly asymmetric distribution or hardening pressure processes. It is worth to note that the proposed mixTPP method is limited by the capability of adopted mixture distributions to accurately model non-Gaussian pressure data. The applicability of two-component Weibull mixtures to model general pressure data needs to be further studied in the future.

7. Conclusions

In this paper, high-order moments and peak factors of non-Gaussian pressure process are investigated based on the wind tunnel experiments of a cylindrical reticulated roof structure with or without coal piles inside. The focus is put on the estimation of time-dependent non-Gaussian statistics of long-duration pressure records for three different testing cases, i.e., the empty roof without coal piles, half coal piles inside and full coal piles. It was found that high-order moments of net wind pressure on the shell roof exhibit strong sensitivity to the record duration. The maximum value of COVs (Coefficients of variations) of high-order moments is up to 1.05 for several measured pressure processes. Such a significant dispersion of the estimated high-order moments using the conventional 10-miniute duration pressure data indicates that the moment-base translation method, which is depend on the estimated skewness and kurtosis, would suffer large uncertainty in the estimation of peak wind loads using short-term time history samples. The newly revealed statistical property of wind pressure fields is characterized as non-Gaussian time-dependent statistics, which could lead to a high-order non-stationary process with constant mean and variance.

Various mixture distributions were introduced to describe and model non-Gaussian wind pressure processes, i.e., WW-pdf, NW-pdf and KP-pdf. The results of goodness-of-fit analysis show that both KP-pdf and WW-pdf are quite adequate to model hardening wind pressure process with PPCC values very close to unity. With the aid of mixture distributions, the TPP method has been revised and improved to estimate non-Gaussian peak factors. The comparison of non-Gaussian peak factors estimated by various state-of-the-art methods demonstrates that the MixTPP considering the two-component Weibull mixtures seems quite effective in further improving the accuracy of the current TPP method. The TPP method and its various revisions exhibit their advantages of stability and accuracy over the moment-based translation method in calculating non-Gaussian peak factors. The estimated non-Gaussian peak factors of wind pressure on the long roof with open ends were also found to be sensitive to the presence of coal piles inside, i.e., a hardening pressure process at the leading edge of the roof were varying from 3.6229, 3.3693 to 3.3416 corresponding to three different cases of A, B and C.

Acknowledgements

References

Abhilash, S. and Jeffrey, M.F. (2014), "Non-Gaussian analysis methods for planing craft motion", *Ocean Syst. Eng.*, **4**(4), 293-308.

Akdağ, S.A., Bagiorgas, H.S. and Mihalakakou, G. (2010), "Use of two-component Weibull mixtures in the analysis of wind speed in the Eastern Mediterranean", *Appl. Energ.*, **87**(8), 2566-2573

Bordes, L., Mottelet, S. and Vandekerkhove, P. (2006). "Semiparametric estimation of a two-component mixture model", *Ann. Stat.*, **34**(3), 1204-1232.

Butt, U., Jehring, L. and Egbers, C. (2014), "Mechanism of drag reduction for circular cylinders with patterned surface", *Int. J. Heat. Fluid. Fl.*, **45**, 128-134.

Chen, X. (2014), "Extreme value distribution and peak factor of crosswind response of flexible structures with nonlinear aeroelastic effect", *J. Struct. Eng.*, DOI: 10.1061/(ASCE)ST.1943-541X.0001017, 04014091.

Choi, M. and Sweetman, B. (2010), "The Hermite moment model for highly skewed response with application to tension leg platforms", *J. Offshore. Mech. Arct.*, **132**, 021602.

DeCarlo, L.T. (1997), "On the meaning and use of kurtosis", *Psychol. Methods.*, **2**(3), 292-307.

Ding, J. and Chen, X. (2014), "Assessment of methods for extreme value analysis of non-Gaussian wind effects with short-term time history samples", *Eng. Struct.*, **80**, 75-88.

Filliben, J.J. (1975), "The probability plot correlation coefficient test for normality", *Technometrics*, **17**(1), 111-117

Harris, I. (2005), "Generalised Pareto methods for wind extremes: usefull tool or mathematical mirage?", *J. Wind. Eng. Ind. Aerod.*, **93**, 341-360.

Hastie, T., Tibshirani, R. and Friedman, J.H. (2009), *The elements of statistical learning*, (2nd Ed.), Springer, New York.

Huang, M.F., Lou, W.J., Chan, C.M. *et al.* (2013), "Peak distributions and peak factors of wind-induced pressure processes on tall buildings", *J. Eng. Mech.- ASCE*, **139**(12), 1744-1756.

Huang, M.F., Lou, W.J., Pan, X.T. *et al*. (2014), "Hermite extreme value estimation of non-Gaussian wind load process on a long-span roof structure", *J. Struct. Eng.- ASCE*.

Jiang, Y., Tao, J. and Wang, D. (2014), "Simulation of non-Gaussian stochastic processes by amplitude modulation and phase reconstruction", *Wind Struct.*,**18**(6), 693-715.

Kareem, A. and Zhao, J. (1994), "Analysis of non-gaussian surge response of tension leg platforms under wind loads", *J. Offshore. Mech. Arct. Eng.*, **116**, 137-144.

Kwon, D. and Kareem, A. (2011), "Peak factors for non-Gaussian load effects revisited", *J. Struct. Eng. - ASCE*, **137**(12), 1611-1619.

MacDonald, A., Scarrott, C.J. and Lee, D.S. (2011b), Boundary correction, consistency and robustness of kernel densities using extreme value theory. Available from: http://www.math.canterbury.ac.nz/ c.scarrott.

MacDonald, A., Scarrott, C.J., Lee, D., Darlow, B., Reale, M. and Russell, G. (2011a), "A flexible extreme value mixture model", *Comp. Statist. Data. Anal.*, **55**, 2137-2157.

National Stanadrd of China (2012), Load code for the design of building structures. GB 50009-2012. (in chinese).

Peng, X., Yang, L., Gavanski, E. *et al*. (2014), "A comparison of methods to estimate peak wind loads on buildings", *J. Wind Eng. Ind. Aerod.*, **126**, 11-23.

Sadek, F. and Simiu, E. (2002), "Peak non-Gaussian wind effects for database-assisted low-rise building design", *J. Eng. Mech.- ASCE*, **128**, 530-539.

Tieleman, H.W., Elsayed, M.A.K. and Hajj, M.R. (2006), "Peak wind load comparison: theoretical estimates and ASCE 7", *J. Struct. Eng. – ASCE*, **132**(7), 1150-1157.

Titterington, D.M., Smith, A.F.M. and Makov, U.E. (1995), *Statistical analysis of finite mixture distributions*, (2nd Ed.), New York, Wiley.

Winterstein, S.R. (1988), "Nonlinear vibration models for extremes and fatigue", *J. Eng. Mech. – ASCE*, **114**, 1772-1790.

Winterstein, S.R. and Kashef, T. (2000), "Moment-based load and response models with wind engineering applications", *J. Sol. Energy Eng. T- ASME*, **122**(3), 122-128.

Winterstein, S.R. and MacKenzie, C.A. (2012), "Extremes of nonlinear vibration: models based on moments, L-moments, and maximum entropy", *J.Offshore.Mech. Arct.*, **135**(2), 021602.

Yang, L., Gurley, K.R. and Prevatt, D.O. (2013). "Probabilistic modeling of wind pressure on low-rise buildings", *J. Wind Eng. Ind. Aerod.*, **114**, 18-26.

Zheng, H., Huang, G. and Liu, X. (2014), "Mixture probability distributions of wind pressure on low-rise buildings", *Proceedings of the 2014 World Congress on Advances in Civil, Environmental and Materials Research (ACEM14)*, Busan, Korea, August 24-28.

CC